Design, Synthesis and Biological Evaluation of Novel Benzoylimidazole Derivatives as Raf and Histone Deacetylases Dual Inhibitors

Xin Chen,*[a] Guoliang Gong,[a] Xinyang Chen,[a] Ruihu Song,[a] Mei Duan,[a] Ruizhi Qiao,[a] Yu Jiao,[b] Jianzhao Qi,[a] Yadong Chen,[b] and Yong Zhu[b]

[a] *Shaanxi Key Labotory of Natural Products & Chemical Biology, College of Chemistry & Pharmacy, Northwest A&F University; Yangling 712100, P. R. China: and* [b] *School of Science, China Pharmaceutical University; Nanjing, 210009, P. R. China.*

In recent studies, combinations of histone deacetylases (HDACs) inhibitor with kinase inhibitor showed additive and synergistic effects. BRaf^{V600E} as an attractive target in many diseases treatments has been studied extensively. Herein, we present a novel design approach though incorporating the pharmacophores of BRaf^{V600E} inhibitor and HDACs inhibitor in one molecule. Several synthesized compounds exhibited distinct BRaf^{V600E} and HDAC1 inhibitory activities. The representative dual Raf/HDAC inhibitor, 7a, showed better antiproliferative activities against A549 and SK-Mel-2 in cellular assay than SAHA and sorafenib, with IC$_{50}$ values of 9.11 μM and 5.40 μM, respectively. This work may lay the foundation for the further development of dual Raf/HDAC inhibitors as potential anticancer agents.

Key words   BRaf^{V600E}; histone deacetylase 1 (HDAC1); antiproliferation; dual inbihitor; synthesis

Introduction

During the last few decades, developing mechanism-based targeted anticancer drugs has made great achievement. However, unsustainable clinical effectiveness and acquired drug resistance always limits the use of these agents.[1] Since cancer is a disease involving complex signaling networks, blocking a single biological target may not completely shut off the core hallmark capability, allowing residual cancer cells to go on working. To address these problems, one particularly promising approach is incorporating the elements that simultaneously tackle multiple cancer-fighting targets into one molecule to obtain new chemical entity. Compared to single-target treatment, this kind of therapeutic regimens have superior efficacy and fewer side effects.[2]

Protein kinases are important participants in the processes of governing cellular proliferation, differentiation and evasion from apoptosis. BRaf, as one member of the Raf family, plays a crucial role in the Ras/Raf/Mek/Erk (mitogen-activated protein kinase, MAPK) signaling pathway.[3,4] The Mutation of BRaf, especially BRaf^{V600E}, is the most common in human cancers. Up to data, a lot of BRaf^{V600E} inhibitors have been developed such as sorafenib,[5] dabrafenib, and vemurafenib (Fig. 1). They effectively block the MAPK signaling pathway and inhibit proliferation of tumor cells expressing BRaf^{V600E}. Histone deacetylases (HDACs) are important targets for tumor therapy.[6–9] The HDACs family containing 18 isoforms is categorized into Class I (HDAC1, 2, 3, and 8), Class IIa (HDAC4, 5, 7, and 9), Class IIb (HDAC6 and 10), Class III (sirtuin1–7), and Class IV (HDAC11). Class I, II, and IV HDACs are all zinc-dependent deacetylases, and Class III HDACs are mechanistically distinct from other HDACs, which require nicotine adenine dinucleotide as a cofactor. The pharmacophore of HDACs inhibitors were generally composed of three parts: cap, linker, and zinc binding group (ZBG). Hydroxamic acid is the most frequently used ZBG group, three of which (*i.e.*, vorinostat,[10] belinostat,[11] panobinostat[12]) have gained U.S. Food and Drug Administration approvals for clinical treatment.

A lot of literatures have described the synergistic and additive effects by the joint use of HDACs inhibitors and vari-
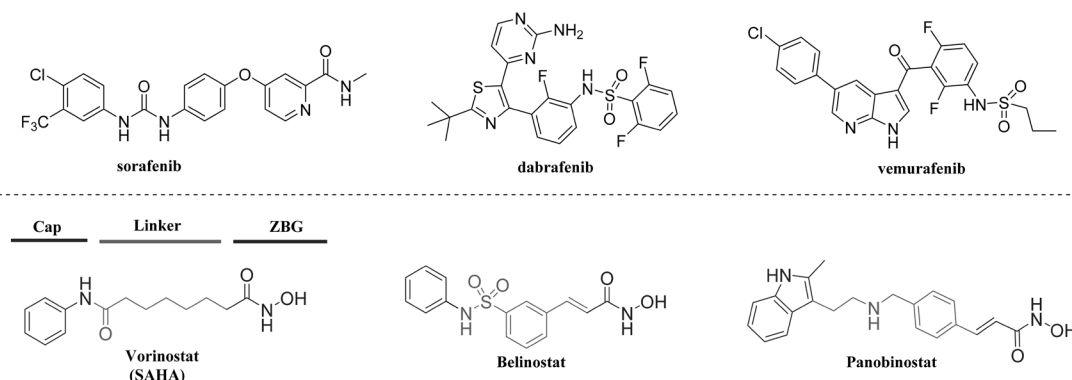

Fig. 1.   Representative BRaf^{V600E} and HDACs Inhibitors

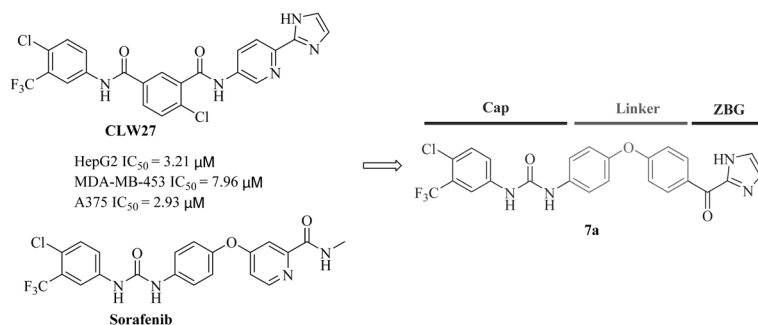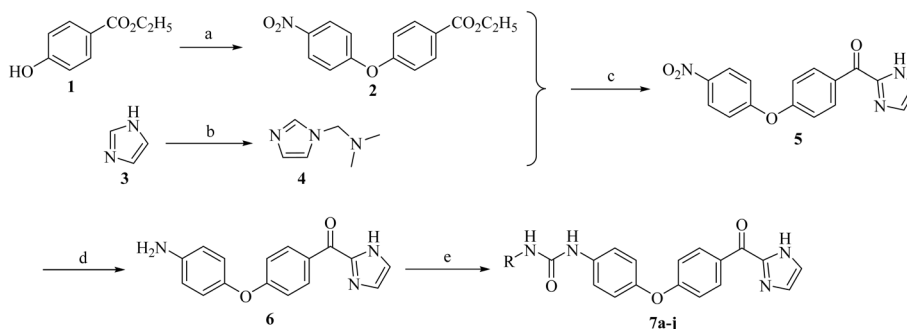* To whom correspondence should be addressed.   e-mail: chenxin1888@nwsuaf.edu.cn

CLW27

HepG2 IC$_{50}$ = 3.21 μM
MDA-MB-453 IC$_{50}$ = 7.96 μM
A375 IC$_{50}$ = 2.93 μM

Sorafenib

Cap Linker ZBG

7a

Fig. 2. Design of Representative Raf/HDAC Dual Inhibitor **7a**

Reagents and conditions: (a) 1-fluoro-4-nitrobenzene, K$_2$CO$_3$, CH$_3$CN, Reflux, 4 h; (b) dimethylamine hydrochloride, CH$_2$O, H$_2$O, HCl, r.t., 48 h; (c) *n*-BuLi, THF, −78°C, 4 h; (d) iron powder, NH$_4$Cl, H$_2$O, C$_2$H$_5$OH, reflux, 4 h; (e) CDI, CH$_2$Cl$_2$, r.t. 12 h, then R-NH$_2$, overnight.

Chart 1.

ous antitumor agents.[13–15] Recently, Emmons *et al.* revealed that HDACs inhibitor could enhance the durability of BRaf inhibitor therapy.[16] Hence, the development of BRaf^{V600E} and HDACs dual inhibitors maybe a valuable strategy to circumvent resistance. Our group had previously reported a 2-(1*H*-imidazol-2-yl) pyridine derivative **CLW27** possessing comparable antiproliferative activities to sorafenib *in vitro* or *in vivo*, and it showed inhibitory effect on BRaf and KDR-VEGFR2 kinases.[17] In that compound, imidazole motief in the hinge region played a beneficial role for antitumor potency. For another, considering the genotoxicity of hydroxamic acid group and generated chromosomal aberrations in many cases,[18,19] an alternative to hydroxamate as ZBG was tried in our design of novel Raf/HDAC dual inhibitors. Vasudevan *et al.* reported the use of acyl imidazole as ZBG in HDAC inhibitors, but it did not show potent inhibitory activity.[20] However, the HDAC activity is not be determined only by the ZBG group, the spatial structures of cap and linker parts also have influence on activity. In this study, we incorporated acyl imidazole motif as ZBG and retained key urea group in sorafenib, then synthesized a series of novel derivatives (Fig. 2).

Chemistry

Compounds **7a–h** were synthesized as follows. Nucleophilic reaction of ethyl 4-hydroxybenzoate (**1**) with 1-fluoro-4-nitrobenzene yielded intermediate **2** using potassium carbonate with acetonitrile as solvent. Compound **4** was obtained by mannich reaction with imidazole (**3**), formaldehyde and dimethylamine hydrochloride as materials. Nucleophilic addition of **2** and **4** in tetrahydrofuran yielded key intermediate **5** with *n*-BuLi as the base. Subsequently, reduction of **5** with iron powder as catalyst in ethanol afforded **6**. Reaction of **6** with
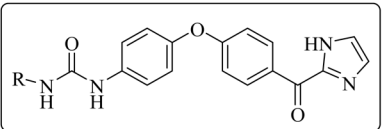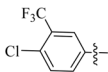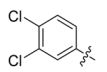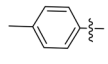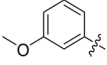
various arylamines in the presence of 1,1′-carbonyldiimidazole at room temperature gave the target compounds **7a–h** (Chart 1).

Results and Discussion

Enzymatic Activities and Structure–Activity Relationship (SAR) Study of Target Compounds The antitumor effect of the inhibition of the class I HDAC isoforms, especially HDAC1, was well confirmed.[21–23] Therefore, all prepared derivatives were tested for their inhibitory ability against HDAC1, using SAHA as the reference compound. As shown in Table 1, IC$_{50}$ values illustrated that compound **7c** bearing a terminal 4-methoxylphenyl, exhibited the best inhibitory activity against HDAC1 (IC$_{50}$ = 635 nM). However, it 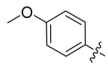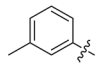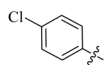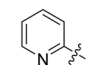was much weaker than that of SAHA. While changing methoxyl from *para*-position to *meta*-position, compound **7f** also showed a comparative activity (IC$_{50}$ = 679 nM). Additionally, compounds with groups such as −Me (**7b**, **7g**), −Cl or −CF$_3$ (**7a**, **7d**, and **7e**) on phenyl inhibited HDAC1 with IC$_{50}$ values in submicromolar or micromolar range. The activities against BRaf^{V600E} of these derivatives were also evaluated. **7a**, which reserved the same 4-chloro-3-trifluoromethyl substituent as sorafenib, had the strongest activity (IC$_{50}$ = 86 nM), although it was slightly less potent than sorafenib (IC$_{50}$ = 38 nM). Compound **7d** and **7e** with electron-withdrawing substitutions also showed moderate inhibitory activities. However, electron-donating substitutions such as -Me or -OMe, were detrimental to BRaf^{V600E} inhibition, exemplified by **7b**, **7c**, **7f**, and **7g**, with IC$_{50}$ values ranging from 0.840 to 4.727 μM. When the phenyl was replaced with pyridyl, obvious declines on both enzymatic activities were observed.

Raf and HDAC Isoforms Selectivity of Representative

Table 1. Enzymatic Inhibitory Activities of Target Compounds **7a–h** (IC$_{50}$^{a}, μM)

Cpd.	R	BRaf^{V600E}	HDAC1	Cpd.	R	BRaf^{V600E}	HDAC1
7a	F$_3$C / Cl phenyl	0.086	1.710	**7e**	Cl Cl phenyl	0.135	1.680
7b	methylphenyl	0.840	0.882	**7f**	methoxyphenyl	4.727	0.679
7c	methoxyphenyl	1.853	0.635	**7g**	methylphenyl	2.032	0.925
7d	Cl phenyl	0.221	1.850	**7h**	pyridyl	>10	4.030
Sorafenib	/	0.038	/	**SAHA**	/	/	0.017

^{a}We ran experiments in duplicate, SD <15%.

Table 2. Raf and HDAC Isoforms Selectivity of Compounds **7a** and **7c** (IC$_{50}$$^{a)}$, μM)

Cpd.	ARaf	BRaf^{V600E}	BRaf^{WT}	CRaf	HDAC1	HDAC6	HDAC8
7a	0.045	0.086	0.134	0.102	1.710	NA$^{b)}$	NA
7c	1.103	1.853	0.226	2.374	0.635	NA	NA
Sorafenib	0.010	0.038	0.024	0.041	/	/	/
SAHA	/	/	/	/	0.037	0.026	3.21

a) We ran experiments in duplicate, S.D. <15%. *b*) NA: no activity was observed at 50 μM concentration.

Compounds Based on the enzymatic results, representative compounds **7a** and **7c** with better HDAC1 or BRaf^{V600E} activity were further evaluated against Raf and HDAC isoforms. As shown in Table 2, **7a** also exhibited potent ARaf, BRaf^{WT}, and CRaf inhibitions. However, **7a** and **7c** showed no activities against HDAC6 and HDAC8.

The most potent compound **7a** was further tested against another six kinases which were frequently used in our lab to evaluate its selectivity and to discovery potential other molecular targets. The initial screening of **7a** was conducted at 10 μM concentration for the inhibitory rates. As summarized in Table 3, compound **7a** showed weak inhibitory effects against KDR-VEGFR2 and EGFR with IC$_{50}$ values of 19.210 μM and 35.470 μM, respectively, and had no obvious inhibition against CDK4/6, FLT3, and BCR/ABL kinases.

Cell Proliferation Inhibition We chose compounds **7a**, **7b**, **7c**, and reference compounds sorafenib and SAHA to evaluate antiproliferative activities against tumor cell lines K562 (leukemia), HCT116 (colon cancer) and A549 (non-small cell lung cancer). As shown in Table 4, all three compounds demonstrated obvious antiproliferative activities against all tumor cells, especially **7a**, although it had the weakest HDAC1 inhibition. Compared to sorafenib, **7a** showed overall more potent antiproliferative activity. **7a** also exhibited superior activity in solid tumor cell line A549 (IC$_{50}$ = 9.11 μM) to that of SAHA (IC$_{50}$ = 18.13 μM). Besides, **7a** was further tested against an-

Table 3. Kinase Inhibitory Effects of Compound **7a**

Kinase	Inhibition rate%	IC$_{50}$ (μM)
KDR-VEGFR2	41.75%	19.210
CDK4/cyclin D1	0.08%	/
CDK6/cyclin D1	−2.05%	/
FLT3	9.20%	/
BCR-ABL	−0.13%	/
EGFR	38.60%	35.470

other two tumor cells SK-Mel-2 (malignant melanoma) and MV4-11 (leukemia) which had extraordinary expression of BRaf^{V600E} or BRaf^{WT}. **7a** displayed submicromolar inhibiton toward MV4-11 with IC$_{50}$ value of 0.38 μM. Especially, **7a** had more potent activity against SK-Mel-2 than those of SAHA and sorafenib.

Molecular Docking Study To further understand the interaction between the inhibitors and two proteins, we docked **7c** in the active site of HDAC1 (PDB code: 5ICN) and **7a** in BRaf^{V600E} (PDB code: 1UWJ) respectively. As shown in Fig. 3A, **7c** exhibited excellent shape complementarity with the binding pocket of HDAC1. The acyl imidazole moiety could form bidentate coordination with zinc ion at the bottom of the pocket, with O-Zn^{2+} distance of 2.510 Å for C=O and N-Zn^{2+} distance of 2.731 Å for imidazole –NH–, respectively. Addi-

Table 4. Antiproliferative Activities of **7a**, **7b**, and **7c** (IC$_{50}$[a], μM)

Cpd.	K562	HCT116	A549	SK-Mel-2	MV4-11
7a	9.13	10.87	9.11	5.40	0.38
7b	12.09	14.24	16.25	/	/
7c	10.10	11.26	13.37	/	/
SAHA	0.65	6.21	18.13	8.20	0.11
Sorafenib	11.20	12.25	10.63	9.30	0.42

a) IC$_{50}$ values are averages of three independent experiments, S.D.<15%.
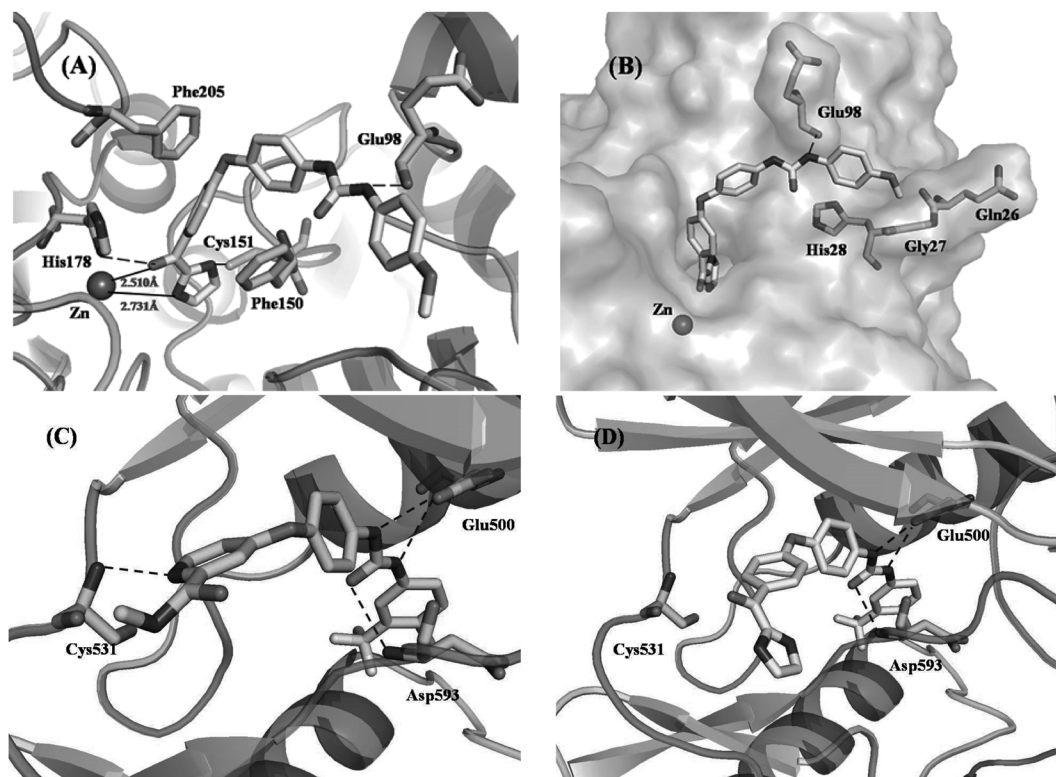

Fig. 3. (A) Docking Model of **7c** (Yellow) in the Catalytic Pocket of HDAC1, with Key Residues in the Hydrophobic Channel Labeled in Green

The zinc ion appears as a large gray sphere. Metal coordination between inhibitor and the catalytic zinc ion were shown in solid black lines. The H-bonding interactions with residues were labeled in dash line; (B) Docked position obtained for **7c** in HDAC1. The HDAC1 protein was shown as a surface representation in gray. (C) The binding mode of sorafenib (wathet) in BRaf^{V600E}; (D) The binding mode of **7a** in BRaf^{V600E}. For clarity, all hydrogen atoms were hidden.

tionally, the O atom of carbonyl and the N atom of imidazole generated H-bond interactions with His178 and Cys151. Moreover, the phenyl linkage connected to acyl imidazole formed stacking π–π interactions with the residues of Phe150 and Phe205. The urea group and two adjacent phenyls occupied the surface groove and came into close contact with the residues (Gln26, Gly27, and His28) at the rim region. Another H-bond was formed between NH of urea and Glu98 to enhance their binding (Fig. 3B). Comparing the binding modes of sorafenib (Fig. 3C) and **7a** (Fig. 3D) in BRaf^{V600E}, **7a** reserved three key H-bond interactions between the urea group and the residues of Glu500 and Asp593, while the H-bond in the hinge was missed. This might be responsible for reduced potency against BRaf^{V600E} of **7a**.

Conclusion

In summary, we designed a series of novel Raf/HDAC dual inhibitors bearing acyl imidazole as ZBG. Eight target compounds were synthesized and tested against BRaf^{V600E} and HDAC1, and most compounds exhibited obvious inhibi-

tory activities. Among these, compounds **7a** and **7c** were the most potent compounds against BRaf^{V600E} and HDAC1, respectively. Then **7a** and **7c** were submitted to evaluate the isoforms selectivities. The results showed these derivatives to be pan-Raf and selective HDAC1 inhibitors. Further *in vitro* antiproliferative assay showed that **7a**, **7b**, and **7c** had inhibitory effects against several tumor cell lines including K562, HCT116, and A549. Moreover, **7a** exhibited more potent antiproliferative activities against A549 and SK-Mel-2 cell lines than sorafenib and SAHA. Subsequently, molecular docking was performed to explain the structure–activity relationship. The demonstration of dual Raf/HDAC inhibitors in this paper provided useful tool compounds for further studies of multiple pathway inhibition achieved with a single molecule.

Experimental

Chemistry All of the starting materials were obtained commercially and were used without further purification. All of the reported yields were for isolated products and were not optimized. Melting points were determined in open capillaries

on a WRS-1A digital melting point apparatus (Shenguang). ^{1}H-NMR spectra was recorded in dimethyl sulfoxide (DMSO)-d_6 on a Bruker DRX-500 (500 MHz) using TMS as internal standard. The chemical shifts were reported in ppm (δ) and coupling constants (J) values were given in Hertz (Hz). Mass spectra were obtained from Agilent 1100 LC/MSD (Agilent, U.S.A.) or Q-tof micro MS (Micromass, U.S.A.). The IR spectra were performed on a FTIR-8400S (Shimadzu, Japan) in KBr pellets; the frequencies are expressed in cm^{-1}. The purities of all tested compounds were established by HPLC to be >95.0%. HPLC analysis was performed at room temperature using an Agilent Eclipse XDB-C18 (250 × 4.6 mm) and 20% MeOH/H$_2$O as a mobile phase and plotted at 254 nm.

Ethyl 4-(4-Nitrophenoxy)benzoate (2)

To a solution of ethyl 4-hydroxybenzoate (16.6 g, 0.1 mol), potassium carbonate (55.2 g, 0.4 mol) in anhydrous acetonitrile (300 mL) under nitrogen atmosphere was added fluoro-4-nitrobenzene (15.5 g, 0.11 mol). The mixture was refluxed for 4 h, then filtered. The mixture was concentrated *in vacuo*, then washed with water. The mother liquid was extracted with ethyl acetate (30 mL × 2). The combined organic extracts were dried over anhydrous MgSO$_4$ and concentrated under reduced pressure. The product was obtained as a white solid by chromatography on a silica gel column (24.3 g, 84.4%); mp: 110–112°C. ^{1}H-NMR (500 MHz, DMSO-d_6) δ: 8.57 (dd, $J = 7.0$, 2.5 Hz, 2H), 8.31 (dd, $J = 7.0$, 2.3 Hz, 2H), 7.25–7.89 (m, 4H), 4.23 (q, $J = 7.2$ Hz, 2H), 1.25 (t, $J = 7.2$ Hz, 3H);

1-(1H-Imidazol-1-yl)-N,N-dimethylmethanamine (4)

Imidazole (20.4 g, 0.3 mol) and dimethylamine hydrochloride (26.0 g, 0.3 mol) were added in 50 mL water at 0°C, then conc. hydrochloric acid was added to adjust pH to 4. Then resulting mixture was stirred for 10 min, and formalin (37%, 27 g, 0.33 mol) was added. The resulting mixture was stirred for additional 48 h at room temperature, then 20% KOH solution was added to adjust pH to 10. The reaction mixture was extracted with chloroform (20 mL × 3). The combined organic extracts were dried over anhydrous Na$_2$SO$_4$ and concentrated under reduced pressure. The product was obtained as a liquid (28.4 g, 75.6%). ^{1}H-NMR (500 MHz, DMSO-d_6) δ: 8.03 (s, 1H), 7.53 (d, $J = 1.9$ Hz, 1H), 7.14 (d, $J = 1.8$ Hz, 1H), 4.82 (s, 2H), 2.51 (s, 6H).

(1H-Imidazol-2-yl)(4-(4-nitrophenoxy)phenyl)methanone (5)

Under nitrogen atmosphere, to a solution of **4** (1.25 g, 10 mmol) in THF (40 mL) at −78°C was added n-BuLi 2.5 M solution in n-hexane (4.2 mL), then the resulting mixture was stirred for 1 h at −78°C. A solution of **2** (3.01 g, 10.5 mmol) in THF (10 mL) was added. The mixture was stirred for 4 h at −78°C and monitored end by TLC. The mixture was acidified with 2 N HCl (80 mL) to adjust pH to 6–7 and extracted with ethyl acetate (40 mL × 3). The combined organic extracts were dried over anhydrous Na$_2$SO$_4$ and concentrated under reduced pressure. The product was obtained as a white solid by chromatography on a silica gel column (2.20 g, 71.2%); mp: 177–179°C; ^{1}H-NMR (500 MHz, DMSO-d_6) δ: 13.46 (br, 1H), 8.65 (dd, $J = 7.0$, 2.5 Hz, 2H), 8.31 (dd, $J = 7.0$, 2.3 Hz, 2H), 7.53 (d, $J = 1.9$ Hz, 1H), 7.34–7.29 (m, 5H).

(4-(4-Aminophenoxy)phenyl)(1H-imidazol-2-yl)methanone (6)

To a solution of **5** (2.00 g, 7 mmol), ammonium chloride (0.37 g, 7 mmol) in water (20 mL) and ethanol (1 mL) was added iron powder (3.70 g, 70 mmol) in batches. The mixture

was refluxed for 4 h, then filtered. The mother liquid was extracted with ethyl acetate (20 mL × 3). The combined organic extracts were dried over anhydrous MgSO$_4$ and concentrated under reduced pressure. The product was obtained as a white solid by chromatography on a silica gel column (1.66 g, 85.0%); mp: 192–194°C; ^{1}H-NMR (500 MHz, DMSO-d_6) δ: 13.36 (br, 1H), 8.53 (dd, $J = 8.8$, 2.7 Hz, 2H), 7.48 (s, 1H), 7.27 (s, 1H), 6.97 (d, $J = 8.9$ Hz, 2H), 6.85 (d, $J = 8.7$ Hz, 2H), 6.63 (d, $J = 8.7$ Hz, 2H), 5.08 (s, 2H).

General Procedure for the Preparation of Target Compounds 7a–h

To a solution of **6** (3 mmol) in anhydrous dichloromethane (5 mL) was added CDI (0.58 g, 3.6 mmol) at room temperature. After the mixture was stirred for 12 h, different arylamine (3.6 mmol) was added. The mixture was stirred for overnight. After completion of the reaction as monitored by TLC, the reaction mixture was filtered. The filter cake was washed with CH$_2$Cl$_2$ (2 mL × 2) and dried *in vacuo*. The crude product was recrystallizated in mixed solvent of ethyl acetate and tetrahydrofuran (v/v = 1 : 1) to give the purified target compound.

1-(4-(4-(1H-Imidazole-2-carbonyl)phenoxy)phenyl)-3-(4-chloro-3-(trifluoromethyl)phenyl)urea (7a)

White solid; yield 73.6%; mp: 235–237°C; ^{1}H-NMR (500 MHz, DMSO-d_6) δ: 13.37 (s, 1H), 9.16 (s, 1H), 8.91 (s, 1H), 8.58 (d, $J = 9.0$ Hz, 2H), 8.11 (d, $J = 2.4$ Hz, 1H), 7.66 (dd, $J = 8.8$, 2.4 Hz, 1H), 7.61 (d, $J = 8.8$ Hz, 1H), 7.55 (d, $J = 8.9$ Hz, 2H), 7.49 (d, $J = 2.4$ Hz, 1H), 7.28 (s, 1H), 7.12 (d, $J = 8.9$ Hz, 2H), 7.06 (d, $J = 9.0$ Hz, 2H); ESI-MS *m/z*: 501.1 ([M + H]$^+$), 523.1 ([M + Na]$^+$); IR (KBr, cm^{-1}): 3344, 1674, 163, 1597, 1541, 1489, 1323, 906, 775, 611.

1-(4-(4-(1H-Imidazole-2-carbonyl)phenoxy)phenyl)-3-(p-tolyl)urea (7b)

White solid; yield 75.7%; mp: 246–247°C; ^{1}H-NMR (500 MHz, DMSO-d_6) δ: 13.39 (s, 1H), 8.70 (s, 1H), 8.58 (d, $J = 8.9$ Hz, 2H), 8.55 (s, 1H), 7.53 (d, $J = 8.9$ Hz, 2H), 7.50 (d, $J = 2.4$ Hz, 1H), 7.35 (d, $J = 8.3$ Hz, 2H), 7.28 (s, 1H), 7.12-7.04 (m, 6H), 2.25 (s, 3H); ESI-MS *m/z*: 413.3 ([M + H]$^+$); IR (KBr, cm^{-1}): 3304, 1635, 1603, 1553, 1501, 1302, 1217, 823, 744, 665.

1-(4-(4-(1H-Imidazole-2-carbonyl)phenoxy)phenyl)-3-(4-methoxyphenyl)urea (7c)

White solid; yield 76.1%; mp: 239–240°C; ^{1}H-NMR (500 MHz, DMSO-d_6) δ: 13.39 (s, 1H), 8.67 (s, 1H), 8.57 (d, $J = 8.9$ Hz, 2H), 8.47 (s, 1H), 7.54 (d, $J = 9.0$ Hz, 2H), 7.50 (s, 1H), 7.36 (d, $J = 8.3$ Hz, 2H), 7.28 (s, 1H), 7.10 (s, 2H), 7.05 (s, 2H), 6.88 (d, $J = 8.9$ Hz, 2H), 3.71 (s, 3H); ESI-MS *m/z*: 429.3 ([M + H]$^+$); IR (KBr, cm^{-1}): 3348, 1634, 1591, 1501, 1475, 1389, 1225, 903, 773, 662.

1-(4-(4-(1H-Imidazole-2-carbonyl)phenoxy)phenyl)-3-(4-chlorophenyl)urea (7d)

White solid; yield 70.1%; mp: 268–270°C; ^{1}H-NMR (500 MHz, DMSO-d_6) δ: 13.40 (s, 1H), 8.82 (s, 1H), 8.80 (s, 1H), 8.56 (d, $J = 9.0$ Hz, 2H), 7.54 (d, $J = 8.9$ Hz, 2H), 7.51–7.47 (m, 3H), 7.33 (d, $J = 8.9$ Hz, 2H), 7.28 (s, 1H), 7.10 (d, $J = 8.9$ Hz, 2H), 7.06 (d, $J = 8.9$ Hz, 2H); ESI-MS *m/z*: 433.2 ([M + H]$^+$); IR (KBr, cm^{-1}): 3360, 1686, 1595, 1497, 1389, 1229, 905, 839, 768, 598.

1-(4-(4-(1H-Imidazole-2-carbonyl)phenoxy)phenyl)-3-(3,4-dichlorophenyl)urea (7e)

White solid; yield: 78.1%; mp: 263–265°C; ^{1}H-NMR (500 MHz, DMSO-d_6) δ: 13.38 (s, 1H), 9.00 (s, 1H), 8.88 (s, 1H), 8.57 (d, $J = 9.0$ Hz, 2H), 7.88 (d, $J = 2.4$ Hz, 1H), 7.53 (d,

$J = 9.0$ Hz, 2H), 7.51 (d, $J = 9.0$ Hz, 1H), 7.49 (d, $J = 2.4$ Hz, 1H), 7.35 (dd, $J = 8.9$, 2.5 Hz, 1H), 7.28 (s, 1H), 7.12 (d, $J = 8.9$ Hz, 2H), 7.06 (d, $J = 9.0$ Hz, 2H); ESI-MS *m/z*: 467.2 ([M + H]$^+$); IR (KBr, cm^{-1}): 3348, 1634, 1593, 1543, 1386, 1225, 903, 847, 771, 662.

1-(4-(4-(1*H*-Imidazole-2-carbonyl)phenoxy)phenyl)-3-(3-methoxyphenyl)urea (**7f**)

White solid; yield: 70.7%; mp: 219–221°C; ^{1}H-NMR (500 MHz, DMSO-d_6) δ: 13.36 (s, 1H), 8.72 (s, 1H), 8.66 (s, 1H), 8.58 (d, $J = 9.0$ Hz, 2H), 7.55 (d, $J = 9.0$ Hz, 2H), 7.52 (s, 1H), 7.28 (s, 1H), 7.20–7.19 (m, 2H), 7.12 (d, $J = 8.9$ Hz, 2H), 7.07 (d, $J = 9.0$ Hz, 2H), 6.94 (d, $J = 8.0$ Hz, 1H), 6.55 (d, $J = 7.5$ Hz, 1H), 3.29 (s, 3H); ESI-MS *m/z*: 429.3 ([M + H]$^+$); IR (KBr, cm^{-1}): 3265, 1695, 1572, 1499, 1420, 1393, 1232, 901, 771, 656.

1-(4-(4-(1*H*-Imidazole-2-carbonyl)phenoxy)phenyl)-3-(*m*-tolyl)urea (**7g**)

White solid; yield: 70.2%; mp: 233–235°C; ^{1}H-NMR (500 MHz, DMSO-d_6) δ: 13.38 (s, 1H), 8.72 (s, 1H), 8.58 (s, 1H), 8.56 (d, $J = 9.0$ Hz, 2H), 7.53 (d, $J = 9.0$ Hz, 2H), 7.49 (d, $J = 2.4$ Hz, 1H), 7.30 (s, 1H), 7.28 (s, 1H), 7.23 (d, $J = 9.0$ Hz, 1H), 7.16 (s, $J = 8.0$ Hz, 1H), 7.12 (d, $J = 8.9$ Hz, 2H), 7.05 (d, $J = 9.0$ Hz, 2H), 6.79 (d, $J = 7.5$ Hz, 1H), 2.28 (s, 3H); ESI-MS *m/z*: 413.3 ([M + H]$^+$); IR (KBr, cm^{-1}): 3300, 1639, 1568, 1398, 1240, 906, 847, 775, 658, 517.

1-(4-(4-(1*H*-Imidazole-2-carbonyl)phenoxy)phenyl)-3-(pyridin-2-yl)urea (**7h**)

White solid; yield: 73.9%; mp: 230–232°C; ^{1}H-NMR (500 MHz, DMSO-d_6) δ: 13.40 (s, 1H), 10.61 (s, 1H), 9.47 (s, 1H), 8.58 (d, $J = 8.8$ Hz, 2H), 8.29 (d, $J = 8.0$ Hz, 1H), 7.76 (d, $J = 8.5$ Hz, 1H), 7.62 (d, $J = 8.8$ Hz, 2H), 7.49 (m, 2H), 7.28 (s, 1H), 7.14 (s, 2H), 7.07 (d, $J = 8.9$ Hz, 2H), 7.02 (t, $J = 6.9$ Hz, 1H); ESI-MS *m/z*: 400.3 ([M + H]$^+$); IR (KBr, cm^{-1}): 3275, 1639, 1603, 1558, 1402, 1234, 1159, 908, 849, 773.

***In Vitro* HDAC Enzyme Assay** The HDAC activity was determined using the HDAC fluorimetric activity assay kit (Biomol, Plymouth Meeting, PA, U.S.A.). Briefly, recombinant proteins of HDAC1, 6 and 8 was incubated with test compounds, and HDAC reaction was initiated by addition of Fluor-de-Lys substrate. Samples were incubated for 10 min at room temperature, followed by adding developer to stop the reaction. Fluorescence was measured by a fluorimetric reader with excitation at 360 nm and emission at 460 nm. The HDAC activity was expressed as arbitrary fluorescence units (AFU). The HDAC activity was calculated as a percentage of activity compared with the control group. The IC$_{50}$ values for the test compounds were calculated using SigmaPlot software.

***In Vitro* Kinase Enzyme Assay** Activity of full length BRaf^{V600E} was determined using Hot-Spot^{SM} kinase assay. 5 nM of human GST-tagged BRaf^{V600E} protein (AA416–766) (Invitrogen, Cat# PV3894) was mixed with 20 μM of the substrate His 6-Tagged Full-length Human MEK1 (K97R) in reaction buffer (20 mM Hepes pH 7.5, 10 mM MgCl$_2$, 1 mM ethylene glycol bis(2-aminoethyl ether)-*N,N,N′,N′*-tetra acetic acid (EGTA), 0.02% Brij35, 0.02 mg/mL BSA (albumin from bovine serum), 0.1 mM Na$_3$VO$_4$, 2 mM DTT, 1% DMSO at room temperature, the compounds dissolved in 100% DMSO at indicated doses (starting at 30 μM with 3-fold dilution) was delivered into the kinase reaction mixture by Acoustic technology (Echo550; nanoliter range), incubate for 20 min at room temperature. After 10 μM ^{33}P-γ-ATP (specific activity

10 μCi/μL) (Perkin Elmer, NEG302H001 MC) was added to initiate the reaction, the reactions were carried out at 25°C for 2 h. The kinase activities were detected by filter-binding method. IC$_{50}$ values and curve fits were obtained by Prism (GraphPad Software).

The Pan-Raf and other kinases inhibitory assay were in a manner same as BRaf^{V600E}.

Cell Culture and Cytotoxicity/Proliferation Assay The antiproliferative activitives of compounds **7a**, **7b**, and **7c** were evaluated against different tumor cell lines by the standard 3-(4,5-dimethylthiazol-2-yl)-2,5-diphenyltetrazolium bromide (MTT) assay *in vitro*, with SAHA and sorafenib as the positive control. The cancer cell lines were cultured in RPMI 1640 medium with 10% fetal bovine serum (FBS). Approximate 2.5×10^3 cells, suspended in RPMI 1640 medium, were plated into each well of a 96-well plate and incubated in 5% CO$_2$ at 37°C for 24 h. The tested compounds at the indicated final concentrations were added to the culture medium and incubated for 48 h. Fresh MTT was added to each well at the terminal concentration of 0.5 mg/mL, and incubated with cells at 37°C for 4 h. After the supernatant was discarded, 150 μL DMSO was added to each well, and the absorbance values were determined by a microplate reader (Bio-Rad, Hercules, CA, U.S.A.) at 490 nm.

Computational Methods All computational work was performed in Discovery Studio 3.0 software (BIOVIA, 5005 Wateridge Vista Drive, San Diego, CA92121 U.S.A.). Docking was conducted using Cdocker module based on the cocrystal of BRaf^{V600E} (PDB: 1UWJ) and HDAC1 (PDB: 5ICN). Water molecules outside the binding pockets were excluded. The energy minimization for compounds was performed by Powell's method for 1000 iterations using tripos force field and with Gasteiger–Hückel charge. The other docking parameters were kept as default.

Conflict of Interest The authors declare no conflict of interest.

Supplementary Materials The online version of this article contains supplementary materials.

References
1) Hanahan D., Weinberg R. A., *Cell*, **144**, 646–674 (2011).
2) Guerrant W., Patil V., Canzoneri J. C., Oyelere A. K., *J. Med. Chem.*, **55**, 1465–1477 (2012).
3) Ribas A., Flaherty K. T., *Nat. Rev. Clin. Oncol.*, **8**, 426–433 (2011).
4) Rebocho A. P., Marais R., *Oncogene*, **32**, 3207–3212 (2013).
5) Agianian B., Gavathiotis E., *J. Med. Chem.*, **61**, 5775–5793 (2018).
6) Falkenberg K. J., Johnstone R. W., *Nat. Rev. Drug Discov.*, **13**, 673–691 (2014).
7) Weichert W., *Cancer Lett.*, **280**, 168–176 (2009).
8) Khan O., La Thangue N. B., *Immunol. Cell Biol.*, **90**, 85–94 (2012).
9) Gammoh N., Lam D., Puente C., Ganley I., Marks P. A., Jiang X., *Proc. Natl. Acad. Sci. U.S.A.*, **109**, 6561–6565 (2012).
10) Marks P. A., Breslow R., *Nat. Biotechnol.*, **25**, 84–90 (2007).
11) Sawas A., Radeski D., O'Connor O. A., *Ther. Adv. Hematol.*, **6**,

202–208 (2015).

12) Laubach J. P., Moreau P., San-Miguel J. F., Richardson P. G., *Clin. Cancer Res.*, **21**, 4767–4773 (2015).

13) Zhu Y., Ran T., Chen X., Niu J., Zhao S., Lu T., Tang W., *Chem. Pharm. Bull.*, **64**, 1136–1141 (2016).

14) Chen X., Zhao S., Wu Y., Chen Y., Lu T., Zhu Y., *RSC Adv.*, **6**, 103178–103184 (2016).

15) Liang X., Zang J., Li X., Tang S., Huang M., Geng M., Chou C. J., Li C., Cao Y., Xu W., Liu H., Zhang Y., *J. Med. Chem.*, **62**, 3898–3923 (2019).

16) Emmons M. F., Faião-Flores F., Sharma R., Thapa R., Messina J. L., Becker J. C., Schadendorf D., Seto E., Sondak V. K., Koomen J. M., Chen Y. A., Lau E. K., Wan L., Licht J. D., Smalley K. S. M., *Cancer Res.*, **79**, 2947–2961 (2019).

17) Jiao Y., Xin B. T., Zhang Y., Wu J., Lu X., Zheng Y., Tang W., Zhou X., *Eur. J. Med. Chem.*, **90**, 170–183 (2015).

18) Olaharski A. J., Ji Z., Woo J. Y., Lim S., Hubbard A. E., Zhang L., Smith M. T., *Toxicol. Sci.*, **93**, 341–347 (2006).

19) Johnson D., Walmsley R., *Mutat. Res.*, **751**, 96–100 (2013).

20) Vasudevan A., Ji Z., Frey R. R., Wada C. K., Steinman D., Heyman H. R., Guo Y., Curtin M. L., Guo J., Li J., Pease L., Glaser K. B., Marcotte P. A., Bouska J. J., Davidsen S. K., Michaelides M. R., *Bioorg. Med. Chem. Lett.*, **13**, 3909–3913 (2003).

21) Weichert W., Roske A., Gekeler V., Beckers T., Stephan C., Jung K., Fritzsche F. R., Niesporek S., Denkert C., Dietel M., Kristiansen G., *Br. J. Cancer*, **98**, 604–610 (2008).

22) Weichert W., Roske A., Niesporek S., Noske A., Buckendahl A. C., Dietel M., Gekeler V., Boehm M., Beckers T., Denkert C., *Clin. Cancer Res.*, **14**, 1669–1677 (2008).

23) Chen X., Zhao S., Li H., Wang X., Geng A., Cui H., Lu T., Chen Y., Zhu Y., *Eur. J. Med. Chem.*, **168**, 110–122 (2019).